Pergamon

Int. J. Heat Mass Transfer. Vol. 41, No. 10, pp. 1205–1218, 1998

Printed in Great Britain
0017–9310/98 $19.00+0.00

PII: S0017-9310(97)00217-2

Turbulent developing convective heat transfer in a tube for fluids near the critical point

SANG HO LEE and JOHN R. HOWELL†

Department of Mechanical Engineering, The University of Texas at Austin, Austin, TX 78712, U.S.A.

(*Received* 14 *February* 1997 *and in final form* 14 *July* 1997)

Abstract—Numerical simulation is performed to study turbulent convective heat transfer to fluids near the critical point in the entrance region of a vertical tube. This modeling includes the effects of large thermodynamic and transport property variations of the fluid. The effect of proximity to the critical point is also considered as well as the buoyancy force in the vertical tube. Due to the property variation effects and buoyancy force in the tube, there is slow approach to fully developed conditions. The effects of large property variations are considered with a modified mixing length model including density fluctuation. Predictions from the mixing length model are in good agreement with experimental data from the literature and other analyses. The results show a little higher value in turbulent diffusivity than the standard mixing length model. The buoyancy force in the vertical tube depends on fluid temperature and pressure. The buoyancy force parameters increase as the pressure approaches critical pressure due to the steep density gradient with temperature which affects the characteristics of fluid flow and heat transfer in the developing region. The distributions of heat transfer coefficient and friction factor along the tube are quite different from those of the constant property case. © 1998 Elsevier Science Ltd.

1. INTRODUCTION

Heat transfer to fluids near the thermodynamic critical point in flow through circular tubes is of continuing interest. The distinguishing feature is the large variations of the thermodynamic and transport properties that occur near the pseudocritical point. Due to the effect of property variations, heat transfer and flow characteristics are different from those of the constant property case: the differences depend on the particular fluid and the thermal inlet and boundary conditions. The similar case of fluids with variable properties has engendered many experimental and theoretical studies.

These heat transfer phenomena near the critical region have been observed in applications which use fluids such as water, carbon dioxide, helium and hydrogen. Because of the need to design systems such as heat exchangers for use near the critical point, there have been a considerable number of experimental and theoretical investigations of the flow and heat transfer with conventional heat transfer correlations, experimentally obtained correlations for near-critical fluids, and numerical predictions. These works were chiefly concerned with the heat transfer coefficient and wall temperature distribution along a uniformly heated tube, which are useful design parameters. These two parameters show remarkably different characteristics compared to the constant property case due to the very large variation of properties. Although a number of studies have been performed to describe heat transfer near the critical region, the phenomena are not understood completely.

Near the critical point, there are large variations with temperature and pressure in the thermodynamic and transport properties such as density, specific heat, viscosity and conductivity. Figure 1 shows the density and specific heat at constant pressure dependency on temperature for water. As the pressure approaches the critical pressure, these variations become severe. This results from the fact that no boundary exists between the liquid and gas phase.

The temperature where the specific heat attains a maximum for a specified pressure is called the pseudocritical temperature or transposed critical temperature, T_{pc}. This temperature depends on the pressure and Fig. 2 shows the pseudocritical temperature variation with pressure near the critical region as well as the maximum value of specific heat at constant pressure. It can be seen that the pseudocritical temperature has an almost linear relationship with pressure in the pressure range of $1 < P_R < 1.25$. The pseudocritical temperature should have significant effect on the characteristics of fluid flow and heat transfer for a fluid in the critical region due to the steep variation of specific heat as well as other properties. Large changes at constant pressure are also encountered in thermal conductivity and viscosity in the critical region although the effects are relatively small compared with changes in specific heat.

The Prandtl number varies with pressure and temperature near the critical region. Its variation also has

† Author to whom correspondence should be addressed.

NOMENCLATURE

A^*	a constant
C_p	specific heat at constant pressure [J kg^{-1} K]
D	tube diameter [m]
D_t	turbulent viscosity ratio
f	friction factor
g	acceleration due to gravity [m s^{-2}]
G	mass flux [kg m^{-2} s]
Gr	Grashof number $[Gr = g(\rho_{in}-\rho_w)D^3/\rho_{in}\nu_{in}^2]$
h	heat transfer coefficient [W m^{-2} K]
i	enthalpy [J kg^{-1}]
k	thermal conductivity [W m^{-1} K]
K	a constant
l_m	mixing length [m]
L	tube length [m]
N	relaxation factor
P	pressure [Pa]
P_R	reduced pressure ($P_R = P/P_c$)
Pr	Prandtl number
Q	heat flux [W m^{-2}]
r	radial coordinate [m]
R	radius of tube [m]
Re	Reynolds number ($Re = \rho_{in}u_{in}D/\mu_{in}$)
T	temperature [K]
u	velocity in axial direction [m s^{-1}]
v	velocity in radial direction [m s^{-1}]
y	radial distance from the wall [m]
y^+	dimensionless distance from the wall $[y^+ = \sqrt{(\tau_w\rho_w)}y/\mu_w]$
z	axial coordinate [m].

Greek symbols

α	nonuniform parameter
β	compressibility [1/K]
Γ	diffusion coefficient
ε	turbulent diffusivity [m^2 s^{-1}]
θ	nondimensional temperature $[\theta = (T-T_{in})/(T_w-T_{in})]$
λ	a constant
μ	absolute viscosity [kg s^{-1} m]
ν	kinematic viscosity [m^2 s^{-1}]
ρ	density [kg m^{-3}]
τ	shear stress [N m^{-2}]
ϕ	function variable.

Subscripts

b	bulk condition
c	critical point value
fd	fully developed
H	heat
in	inlet condition
M	momentum
new	new value
old	old value
pc	pseudocritical point
t	turbulent flow
w	wall condition.

Superscript

i	iteration number.

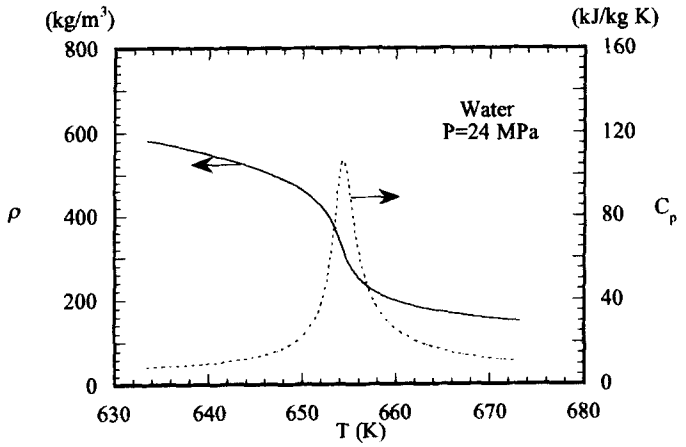

Fig. 1. Density and specific heat variation with temperature for water near the critical point.

a peak at the pseudocritical temperature as for specific heat, and this peak increases as the pressure approaches the critical point. The Prandtl number represents the ratio between momentum diffusivity and thermal diffusivity, and it usually relates the relative thickness of velocity and thermal boundary layers in the constant property case. For fluid flow with heat transfer in the critical region, the Prandtl number is

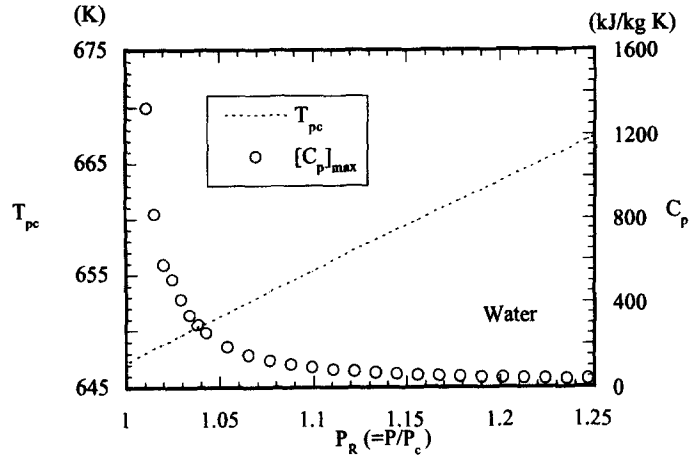

Fig. 2. Pseudocritical temperature variation with pressure and corresponding maximum values of specific heat for water in the critical region.

not constant, but varies with temperature and pressure, which means that the ratio of diffusivities in momentum and energy are locally different.

Related to these property variations, the heat transfer characteristics in a tube for a supercritical fluid show unusual phenomena such as deterioration with gravity and improvement in heat transfer near the pseudocritical temperature. Fundamentally, property variations affect the flow characteristics and these, in turn, affect the heat transfer characteristics. Because of the anomalous behavior of thermodynamic and transport properties for fluids near the critical region, it has been difficult historically to formulate representative correlations which can describe the characteristics of fluid flow and heat transfer over a range of conditions.

Because it provides accurate predictions for certain constant property cases, the k–ε turbulence model is frequently used for supercritical fluids without modification. Most k–ε calculations are based on the model of Jones and Launder [1] and use the same damping function and constants without modification for the steep property variations near the pseudocritical point. This turbulence model works well for normal fluids and is a more general description for turbulence than the mixing length model. In comparison with experimental data, the k–ε predictions are qualitatively correct, but quantitatively there are some discrepancies and they depend on the situation. There is little information about property variation effects on the several coefficients and constants in the equations of kinetic energy and dissipation rate, and the k–ε model is therefore open to question in the present application.

Several studies have solved the equations of motion and energy with a mixing length model of turbulent viscosity. The unusual behavior of the heat transfer coefficient near the critical region was predicted well when compared with experimental data. Bellmore and Reid [2] suggest a method of including the effect of density fluctuation in the equation of turbulent transport. Popov and Valueva [3] also calculated the turbulent viscosity considering density oscillations in the gravity field.

In this investigation, the conservation equations of motion and energy are numerically solved to predict the convection heat transfer phenomena inside a vertical tube for a fluid near the critical region. The effect of proximity to the critical pressure on the heat transfer characteristics is also considered. The mixing length model includes the effect of density fluctuations on turbulent diffusivity. The results are compared with experimental data and calculation results based on k–ε turbulence modeling from the literature.

2. NUMERICAL MODELING

Forced convection heat transfer in a vertical tube is described by the conservation equations of continuity, momentum and energy. Conditions are assumed to be axisymmetric and steady state and the fluid is in local equilibrium for thermodynamic and transport properties calculation. The governing equations of instantaneous form are time averaged and include several standard approximations and turbulence modeling. They are as follows.

Continuity:

$$\nabla \cdot \overline{\rho V} = 0 \tag{1}$$

or

$$\frac{1}{r}\frac{\partial}{\partial r}[r(\overline{\rho v})] + \frac{\partial}{\partial z}(\overline{\rho u}) = 0 \tag{2}$$

where

$$\overline{\rho v} = \overline{\rho}\,\overline{v} + \overline{\rho' v'} \tag{3a}$$

$$\overline{\rho u} = \overline{\rho}\,\overline{u} + \overline{\rho' u'}. \tag{3b}$$

Momentum:

$$\nabla\cdot\overline{\rho VV} = -\nabla P+\overline{\nabla\cdot\tau}+\rho\bar{g} \tag{4}$$

or

r-direction

$$\overline{\rho v}\frac{\partial\bar{v}}{\partial r}+\overline{\rho u}\frac{\partial\bar{v}}{\partial z} = -\frac{\partial\bar{P}}{\partial r}+\frac{1}{r}\frac{\partial}{\partial r}\left[r(\bar{\mu}+\mu_t)\frac{\partial\bar{v}}{\partial r}\right]$$
$$+\frac{\partial}{\partial z}\left[(\bar{\mu}+\mu_t)\frac{\partial\bar{v}}{\partial z}\right]+\frac{1}{r}\frac{\partial}{\partial r}\left\{r\left[\bar{\mu}\left(\frac{\partial\bar{v}}{\partial r}-\frac{2}{3}(\nabla\cdot\bar{V})\right)\right]\right\}$$
$$+\frac{\partial}{\partial z}\left\{\bar{\mu}\left(\frac{\partial\bar{u}}{\partial r}\right)\right\}-\frac{\bar{\mu}}{r}\left[2\frac{\bar{v}}{r}-\frac{2}{3}(\nabla\cdot\bar{V})\right] \tag{5a}$$

z-direction

$$\overline{\rho v}\frac{\partial\bar{u}}{\partial r}+\overline{\rho u}\frac{\partial\bar{u}}{\partial z} = -\frac{\partial\bar{P}}{\partial z}+\frac{1}{r}\frac{\partial}{\partial r}\left[r(\bar{\mu}+\mu_t)\frac{\partial\bar{u}}{\partial r}\right]$$
$$+\frac{\partial}{\partial z}\left[(\bar{\mu}+\mu_t)\frac{\partial\bar{u}}{\partial z}\right]+\frac{1}{r}\frac{\partial}{\partial r}\left[r\bar{\mu}\left(\frac{\partial\bar{v}}{\partial z}\right)\right]$$
$$+\frac{\partial}{\partial z}\left\{\bar{\mu}\left[\frac{\partial\bar{u}}{\partial z}-\frac{2}{3}(\nabla\cdot\bar{V})\right]\right\}+\bar{\rho}g_z \tag{5b}$$

where

$$\nabla\cdot\bar{V} = \frac{1}{r}\frac{\partial}{\partial r}(r\bar{v})+\frac{\partial\bar{u}}{\partial z}. \tag{6}$$

Energy:

$$\nabla\cdot\overline{\rho Vi} = \nabla\cdot\left[\left(\frac{\mu}{Pr}+\frac{\mu_t}{Pr_t}\right)\nabla i\right]$$
$$-\nabla\cdot\left\{\left[\frac{(1-\beta T)k}{\rho C_p}\right]\nabla P\right\}+\frac{DP}{Dt}+\mu\Phi \tag{7}$$

or

$$\overline{\rho v}\frac{\partial\bar{i}}{\partial r}+\overline{\rho u}\frac{\partial\bar{i}}{\partial z} = \frac{1}{r}\frac{\partial}{\partial r}\left[r\left(\frac{\bar{\mu}}{Pr}+\frac{\mu_t}{Pr_t}\right)\frac{\partial i}{\partial r}\right]$$
$$+\frac{\partial}{\partial z}\left[\left(\frac{\bar{\mu}}{Pr}+\frac{\mu_t}{Pr_t}\right)\frac{\partial i}{\partial z}\right]-\frac{1}{r}\frac{\partial}{\partial r}\left[r\frac{(1-\bar{\beta}\bar{T})\bar{k}}{\overline{\rho C_p}}\frac{\partial\bar{P}}{\partial r}\right]$$
$$-\frac{\partial}{\partial z}\left[\frac{(1-\bar{\beta}\bar{T})\bar{k}}{\overline{\rho C_p}}\frac{\partial\bar{P}}{\partial z}\right]+\frac{D\bar{P}}{Dt}+\bar{\mu}\bar{\Phi} \tag{8}$$

where

$$\bar{\Phi} = 2\left[\left(\frac{\partial\bar{v}}{\partial r}\right)^2+\left(\frac{\bar{v}}{r}\right)^2+\left(\frac{\partial\bar{u}}{\partial z}\right)^2\right]+\left(\frac{\partial\bar{v}}{\partial z}+\frac{\partial\bar{u}}{\partial r}\right)^2$$
$$-\frac{2}{3}\left[\frac{1}{r}\frac{\partial}{\partial r}(r\bar{v})+\frac{\partial\bar{u}}{\partial z}\right]^2. \tag{9}$$

In turbulent flow for fluids near the critical point, unlike laminar flow, modeling should include important property variation effects on the fluctuation terms. The effects of thermophysical property variations on these fluctuations are not known well. In this study, the turbulent flow model follows the fluctuating density model proposed by Bellmore and Reid [2]. In this model, density fluctuations with variation of enthalpy are considered and these fluctuations are included in the governing continuity, momentum, and energy equations. Other property fluctuation terms related to diffusivities in the momentum and energy equations, such as dynamic viscosity and thermal conductivity, are neglected as in Hall [4]. In the energy equation, the pressure fluctuation work terms and viscous dissipation terms due to viscosity fluctuation are assumed small compared to the mean value.

For calculation of turbulent transport, the turbulent viscosity and turbulent Prandtl number must be determined. For fluids near the critical region, most of the numerical (theoretical) studies use the same volume of turbulent Prandtl number as for the constant property case because there is little information about property variation effects on turbulent Prandtl number. The turbulent Prandtl number $\varepsilon_M/\varepsilon_H$ is assumed to be 0.9 following previous numerical studies [5, 6]. The modified turbulent eddy viscosity model with Prandtl's mixing length concept [2] is used in this study. This model includes the effect of density fluctuations on turbulent transport characteristics and is expressed as:

$$\mu_t = \rho l_m^2\left|\frac{\partial u}{\partial y}\right|\left[1-\left(\frac{\beta}{C_p}\frac{l_m}{Pr_t}\frac{\partial i}{\partial y}\right)-\left(\frac{\beta}{C_p}\frac{l_m}{Pr_t}\frac{\partial i}{\partial y}\right)^2\right]. \tag{10}$$

This implies that turbulent transport due to density fluctuation is related to the enthalpy gradient and fluid properties. This turbulent viscosity model is based on mean field closure; all variables are time averaged mean values.

Relationships for the mixing length are:

$$l_m = l'[1-\exp(-u_\tau y/v_w A^*)] \tag{11}$$

where

$$l' = K(R-r) \quad \text{for} \quad K(R-r) < \lambda R \tag{12a}$$

$$l' = \lambda R \quad \text{for} \quad K(R-r) > \lambda R. \tag{12b}$$

This follows the empirical two layer model [7] with $K = 0.44$, $\lambda = 0.09$, and $A^* = 26$ for an inner and outer region. The mixing length is based on the Van Driest [8] approach with a damping function.

Considering the effect of enthalpy (temperature) variation, the density fluctuation becomes:

$$\rho' \approx \left(\frac{\bar{\rho}\bar{\beta}l_m}{\overline{C_p}\,Pr_t}\right)\frac{\partial\bar{i}}{\partial y}. \tag{13}$$

The time-averaged value of instantaneous density × velocity product includes the fluctuation aver-

age of mass velocity terms such as $\overline{\rho' v'}$ and $\overline{\rho' u'}$. These terms can be assumed to be of the form [8–10]:

$$\overline{\rho' v'} = C_1 |\rho'| \cdot |v'| \tag{14a}$$

$$\overline{\rho' u'} = C_2 |\rho'| \cdot |u'|. \tag{14b}$$

Little is known about the values of the constants of C_1 and C_2. If these constants are absorbed into the mixing length and turbulent Prandtl number, the magnitude of the two fluctuation product average terms can be expressed as:

$$|\overline{\rho' u'}| = \left| \left(\frac{\bar{\rho} \bar{\beta} l_m^2}{\overline{C_p} Pr_t} \frac{\partial \bar{u}}{\partial y} \frac{\partial \bar{i}}{\partial y} \right) \right| \tag{15a}$$

$$|\overline{\rho' v'}| = \left| \left(\frac{\bar{\rho} \bar{\beta} l_m^2}{\overline{C_p} Pr_t} \frac{\partial \bar{u}}{\partial y} \frac{\partial \bar{i}}{\partial y} \right) \right|. \tag{15b}$$

Whether these values are positive or negative can be decided by observing that the typical average value of $\overline{u' v'}$ near the wall is negative.

It is assumed that the thermal conductivity of the tube wall is very high. Hence, radial and axial thermal resistances of the tube are neglected. Because of the assumed axisymmetric characteristics of heat transfer and flow, half of the tube section in the physical plane is considered.

The associated boundary conditions for the tube flow are as follows.

Inlet:

$$u = u_{in}, \quad v = 0, \quad T = T_{in}, \quad P = P_{in}. \tag{16}$$

Centerline ($r = 0$):

$$\frac{\partial u}{\partial r} = 0, \quad \frac{\partial v}{\partial r} = 0, \quad \frac{\partial i}{\partial r} = 0. \tag{17}$$

Wall ($r = R$):

$$u = 0, \quad v = 0, \quad T = T_w \quad \text{or} \quad Q_w = k \frac{\partial T}{\partial r}\bigg|_{r=R}. \tag{18}$$

At the exit boundary of the tube ($L = 30D$), the linear extrapolation boundary condition is used for the variables. The effect of this boundary condition on the solution near the tube entrance is checked by comparison with calculation results for longer tubes.

Here we examine the case where the wall temperature is higher than the pseudocritical temperature at the inlet pressure and the inlet fluid temperature is lower than the pseudocritical temperature. Hence, the pseudocritical point is located between the wall and centerline of the tube.

Properties are calculated with the program of Lester *et al.* [11] for water and Hendricks *et al.* [12] for CO_2.

3. SOLUTION PROCEDURE

The governing conservation equations can be expressed in the following common form:

$$\frac{\partial}{\partial z}(\rho u \phi) + \frac{1}{r} \frac{\partial}{\partial r}(r \rho v \phi) = \frac{1}{r} \frac{\partial}{\partial r}\left(r \Gamma \frac{\partial \phi}{\partial r} \right) + \frac{\partial}{\partial z}\left(\Gamma \frac{\partial \phi}{\partial z} \right) + S_\phi \tag{19}$$

where ϕ is a general dependent variable and S_ϕ is the source term. The governing general finite difference equations for continuity, momentum, and energy are solved iteratively with the renewal of fluid properties based on the pressure and temperature with the SIMPLE [13] solution algorithm until convergence is achieved for all variables. The staggered grid system is used. In this grid system, each scalar variable such as the pressure, enthalpy (temperature), and properties is defined at the element center. Velocity components are defined at the surfaces of the element. The convergence is checked by solving the governing equations of continuity, momentum, and energy. When the velocities and enthalpy satisfy the convergence criteria:

$$\left| \frac{\phi^{i+1} - \phi^i}{\phi^i} \right| < 10^{-3}; \quad \phi = u, \ v \text{ and } i \tag{20}$$

a converged solution is obtained for the specified grid system.

Relaxation factors are used for stability of convergence with values of 0.5–0.75 for velocities u and v in the momentum equations, and for enthalpy in the energy equation. All thermodynamic and transport properties are also renewed iteratively with an underrelaxation factor (0.25–0.5) as in the following equation:

$$\rho_{new} = (1 - N_{Relaxation}) \rho_{old} + N_{Relaxation} \rho_{new}. \tag{21}$$

The underrelaxation for properties causes the velocity and temperature fields to respond rather slowly to changes in properties due to variation in temperature and pressure. As the pressure inside the tube approaches the critical pressure, a low value of relaxation factor is used in order to prevent divergence.

The low-Reynolds-number turbulence model is used in this study as in other theoretical studies for fluids near the critical point. The use of the wall function which is usually used in the constant property case includes the assumption of a logarithmic layer near the wall. This lets the first grid point be located at $y^+ > 20$–30. The validity of this assumption cannot be verified and it depends on the thermal conditions near the wall for fluids near the critical point. This assumption can be wrong if there are large variations in fluid properties and therefore wall functions are not applied here. The grid should be very fine near the wall in order to apply Couette flow conditions in the laminar sublayer ($y^+ < 5$). For this calculation, a uniform axial grid and an orthogonal nonuniform radial grid which begins with very small increments at the wall and becomes progressively larger toward the center of the tube is used. The grid point adjacent to

the wall is determined such that the nondimensional distance from the wall y^+ is about 1 while typically 80–100 grid points are used for a tube flow. The following relation is used in the radial grid system:

$$y = \frac{(\alpha+1)-(\alpha-1)\{[(\alpha+1)/(\alpha-1)]^{1-\bar{y}}\}}{[(\alpha+1)/(\alpha-1)]^{1-\bar{y}}+1} \quad (22)$$

where $\bar{y}$ is the uniformly distributed radial grid system. The value of the nonuniformity parameter, α, is 1.002–1.005 in the calculation. Numerical accuracy is checked by increasing the number of grid points to properly represent the characteristics of flow and heat transfer.

4. RESULTS AND DISCUSSION

Numerical simulation results for turbulent flow in a tube based on a mixing length model for turbulent diffusivity which includes the effect of density fluctuation in the equation of turbulent transport are shown for fluids in the vicinity of the critical point. Some of the results are compared with those of other experimental and theoretical studies. The effects of thermodynamic and transport property variations on fluid flow and heat transfer including buoyancy force in the developing region of a tube are discussed in this section.

4.1. *Comparison with other predictions and experimental data*

Numerical results are presented in this section for comparison with other analyses and with sparse experimental data. Due to the difficulties in the experiment, there have been few measurements inside a tube of velocity and temperature profiles. Hence, the bulk temperature of the supercritical fluid inside the tube is usually obtained from the heat balance between the wall heat flux and the bulk enthalpy increase of the fluid. This is based on the hypothesis that the bulk enthalpy increase of the fluid in the tube is much larger than changes of kinetic and potential energy or the axial heat diffusion at each end of the tube.

A comparison of the predicted results of this modeling with the experimental data of Wood and Smith [14] for the upward flow of CO_2 is shown in Fig. 3. It shows the comparison of nondimensional profiles of

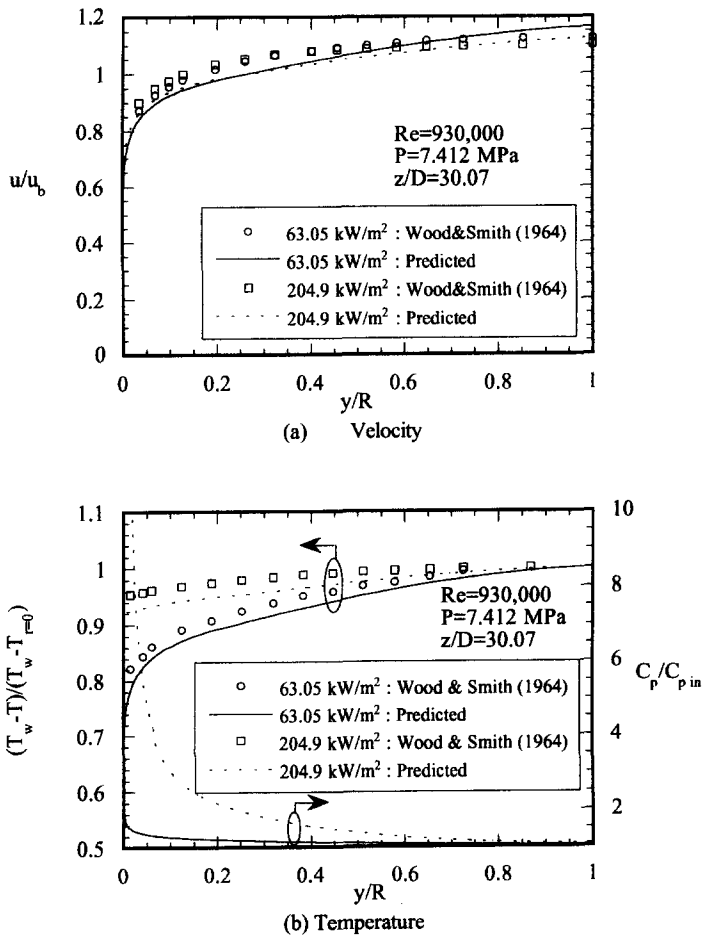

Fig. 3. Comparison of predicted profiles of nondimensionalized velocity and temperature in the tube with experimental data of Wood and Smith [14] for CO_2: (a) velocity; and (b) temperature.

Table 1. Comparison of calculated results of heat transfer coefficient, bulk and wall temperatures with experimental data of Wood and Smith (1964) [14]

	$Q_w = 63.05$ kW m^{-2}		$Q_w = 204.91$ kW m^{-2}	
Parameters compared	Wood and Smith	Calculated	Wood and Smith	Calculated
T_b [K]	302.8	303.0	303.2	303.5
T_w [K]	305.8	305.6	327.4	323.2
h [kW m^{-2} K]	21.45	23.88	8.46	10.62

velocity and temperature for two different wall heat fluxes at the same axial location of a tube. Because of the high mass flow rate ($Re_{in} = 9.3 \times 10^5$), the pseudo-critical point is positioned near the wall, and property variations are very severe near this point. Calculation results based on the mixing length model agree well with the experimental data of Wood and Smith [14]. For both wall heat fluxes, the numerical prediction is in good agreement with experimental data. The velocity and temperature profiles become relatively flatter in the core region of the tube for higher wall heat flux ($Q_w = 204.9$ kW m^{-2}). Wood and Smith [14] suggest that the increase in C_p in the core region for higher heat flux leads to better turbulent transport causing the profiles to become flatter. They also suggest that lower density and viscosity due to the increase of temperature in the sublayer produce the steep velocity gradients near the wall. Heat transfer coefficients along with wall and bulk fluid temperatures for these cases are compared in Table 1. Temperatures measured by Wood and Smith [14] are said to be sensitive within about 0.02 K (0.03°F), although experimental uncertainty was not reported.

The heat transfer coefficient is considerably affected by the wall heat flux. It is reduced to 40% of its value at the higher heat flux. This reduction is due to the decrease of thermal conductivity of the fluid at the tube wall high heat flux. The comparison shows that the predicted heat transfer coefficients are higher than the experimental data. The differences in heat transfer coefficients depend on the wall heat fluxes and for both wall heat fluxes are less than 20%.

In calculation of the mixing length, the non-dimensional distance from the wall y^+ can also be calculated to include the effect of variable properties using the following equations:

$$y^+ = \int_0^y \frac{\sqrt{\rho \tau_w}}{\mu} \mathrm{d}y \tag{23a}$$

$$y^+ = \frac{\sqrt{\rho \tau_w}}{\mu} y. \tag{23b}$$

Equation (23a) is from Goldman [15], and in equation (23b), local property values of density and viscosity are used as in Sastry and Schnurr [16]. Results for the nondimensionalized velocity and temperature distributions obtained using equations (23a) and (23b) in the present calculation are compared near the wall. The differences in predicted velocities are very small, although differences in temperatures can be seen from $y/R < 0.001$ and they become larger close to the wall. The predicted temperature using equation (23a) is a little lower than for equation (23b) and the present prediction. The corresponding heat transfer coefficients obtained from equations (23a) and (23b) are 10.89 kW m^{-2} K and 10.59 kW m^{-2} K at the same axial position. Compared with the results of Table 1, there is less than about 3% difference in the predicted heat transfer coefficients for this condition.

Comparisons with other numerical predictions based on a mixing length model are shown in Fig. 4 for upward flow with constant wall heat flux condition. Popov and Valueva [3] showed the predicted velocity and temperature profiles based on the mixing length model with the boundary layer approximations. This mixing length model includes the effect of density fluctuations on turbulent transfer in a body force field such as gravity. Turbulent stress and heat flux are assumed to be of the form:

$$-\rho \overline{u'v'} = \rho \nu_t \frac{\partial u}{\partial r} - \frac{\beta g^*}{C_p Pr_t} l_m^2 \frac{\partial i}{\partial r} \tag{24}$$

$$-\rho \overline{u'i'} = \rho \frac{\nu_t}{Pr_t} \frac{\partial i}{\partial r}. \tag{25}$$

When the velocity gradient in the radial direction becomes zero in the flow with a gravity force, the turbulent stress term has a nonzero value if there is a nonzero temperature or enthalpy gradient.

Results show that fluid near the tube wall accelerates due to buoyancy effects by heat transfer from the wall. Velocity and temperature distributions obtained from both models agree well in the tube although there are some discrepancies in temperature distribution far from the wall. There are larger variations in properties near the wall than in the tube core due to the steep temperature gradient that occurs with a high wall heat flux. The severe variation in properties near the wall dominates momentum and heat transfer in the tube. Hence, slight differences in temperature distributions far from the tube wall do not have a large influence on the velocity distribution in the tube compared with the near wall region.

Simulation results of heat transfer coefficient based

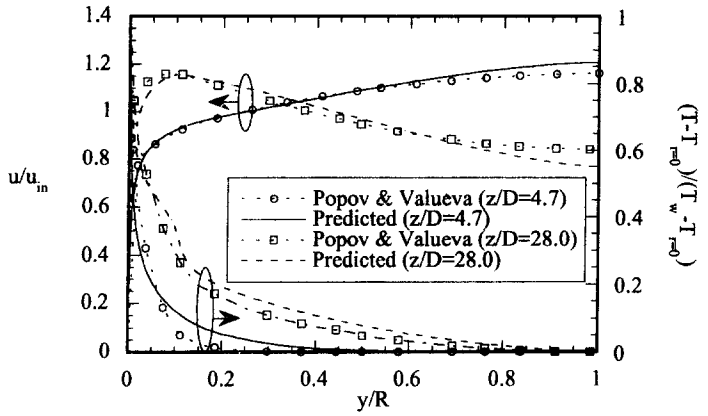

Fig. 4. Comparison of velocity and temperature profiles with results of Popov and Valueva [3]: water ($P = 25$ MPa, $T_{in} = 423$ K, $G = 305$ kg m^{-2} s, $Q_w = 250$ kW m^{-2}).

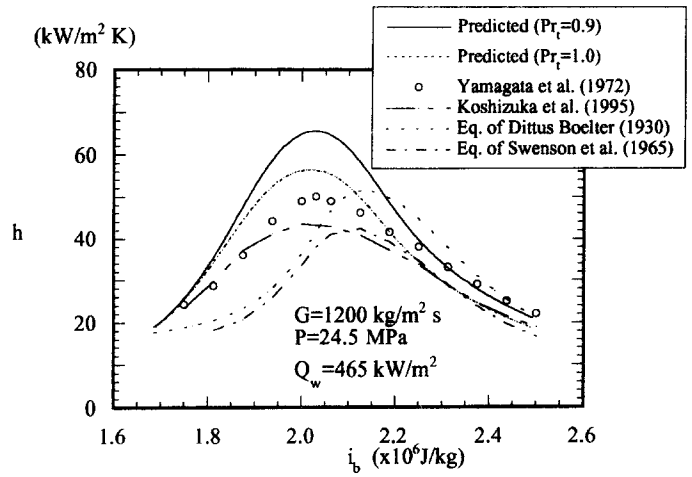

Fig. 5. Heat transfer coefficient distribution along the tube for constant wall heat flux boundary condition: water.

on this modeling are also compared with other data in Fig. 5. They show the predicted heat transfer coefficient variation with bulk enthalpy of fluid along the tube for constant wall heat flux for water, and compare the numerical predictions based on k–ε turbulence modeling [5] and experimental data [17]. The results based on the conventional correlation of heat transfer coefficient using the Dittus–Boelter [18] equation and a modified form proposed by Swenson *et al.* [19] are also compared. These heat transfer coefficients are as follows.

Dittus–Boelter equation [18]:

$$\frac{hD}{k_b} = 0.023\left(\frac{GD}{\mu_b}\right)^{0.8}\left(\frac{C_{p_b}\mu_b}{k_b}\right)^{0.4}. \quad (26)$$

Swenson *et al.* [19]:

$$\frac{hD}{k_w} = 0.00459\left[\frac{GD}{\mu_w}\right]^{0.923} \times\left[\left(\frac{i_w - i_b}{T_w - T_b}\right)\frac{\mu_w}{k_w}\right]^{0.613}\left[\frac{\rho_w}{\rho_b}\right]^{0.231}. \quad (27)$$

Calculation results for the heat transfer coefficient in the developing region of the tube are removed. The calculation result with $Pr_t = 1.0$ is also compared. Near the pseudocritical point (bulk enthalpy = 2.14×10^6 J kg^{-1}), the heat transfer coefficient has a maximum value and as the bulk enthalpy increases above this value, the heat transfer coefficient

decreases. The bulk enthalpies at the peak of the heat transfer coefficient are almost the same for the mixing length and k–ε models as well as for the experimental data, but the bulk enthalpies at the peak of the heat transfer coefficient predicted by the Dittus–Boelter equation and the correlation of Swenson *et al.* [19] are a little higher. The difference between the peaks of the experimental data and the prediction of the Dittus–Boelter equation is relatively small and the prediction of Swenson *et al.* [19] shows a lower peak compared with the result of k–ε modeling. The predicted heat transfer coefficient at the peak by the mixing length models of $Pr_t = 1.0$ and $Pr_t = 0.9$ is about 10 and 31% higher than the experimental data while the result of k–ε modeling is 17% lower.

To predict heat transfer in the supercritical region, the Stanton number determined from the differences of enthalpies is also an important parameter because it includes the influence of variable thermophysical properties. Far from the inlet of the tube ($z/D > 20$–30), the following empirical formula of Stanton number, which is known as Petukhov–Kirillov's equation [20], has been suggested:

$$St = \frac{Q_w}{G(i_w - i_b)} = \frac{f^*/8}{1 + \dfrac{900}{Re_b} + 12.7\sqrt{\dfrac{f^*}{8}}(\overline{Pr}^{2/3} - 1)} \tag{28}$$

where $\overline{Pr}$ is the effective Prandtl number in the wall-adjacent region of the flow in the tube,

$$\overline{Pr} = \left(\frac{i_w - i_b}{T_w - T_b}\right)\frac{\mu_b}{k_b}. \tag{29}$$

The friction factor f^* is described by:

$$\frac{f^*}{f_0} = \left(\frac{\rho_w}{\rho_b}\right)^n \tag{30}$$

where $n = 0.4$ and f_0 is a function of Reynolds number from the Filonenko formula [21]

$$f_0 = [0.55/\log(Re_b/8)]^2. \tag{31}$$

A comparison was made of the results from the above Stanton number correlation and numerical calculations using mixing length theory plus experimental data of Yamagata *et al.* [17]. Near the pseudocritical enthalpy, the Stanton number increases as the bulk fluid enthalpy increases. There is considerable difference between the experimental data and the result based on equation (28), but this difference becomes small as the bulk enthalpy increases above the pseudocritical enthalpy. The results of the mixing length theory agree well with the experimental data.

4.2. *Characteristics in the entrance region of the tube*

Figures 6 and 7 show the comparison of velocity and temperature profiles in the developing region of a tube for no-gravity flow and upward flow of water for the constant wall temperature case with uniform inlet velocity and temperature and $Re = 10^5$. In this case, the wall temperature is higher than the pseudocritical temperature ($T_{pc} = 654$ K for $P = 24$ MPa) and the inlet water temperature is less than the pseudocritical temperature at the pressure in the tube. This condition produces large property variations between the wall and the centerline of the tube. Density, specific heat, viscosity, and conductivity vary severely and their effects on the heat transfer and fluid flow characteristics are interrelated. Hence, it is difficult to say which is the dominant effect. Density variations cause both acceleration of the bulk fluid and increase in the buoyancy force. As the temperature approaches the pseudocritical point, the specific heat increases rapidly compared with other properties such as density and viscosity. This increases the heat transfer by turbulent energy transport even though thermal conductivity decreases with heat transfer. The radial temperature profile is flattened near the pseudocritical temperature. There is a slight flow acceleration along the tube due to density decrease near the wall while severe variation of density is confined close to the wall, and a decrease in viscosity which has the same order of variation with temperature near the pseudocritical point also contributes to the fluid acceleration near the wall. In upward flow, the velocity near the wall increases gradually and smoothly with buoyancy due to density variation. The velocity changes very rapidly near the wall as does the temperature gradient. This effect due to gravity force has a larger influence on momentum transfer in the flow field than just variation of properties such as density and viscosity for convection and diffusion. The effect of buoyancy is seen to be important even at this relatively large value of Reynolds number. The turbulent diffusivity is affected both by the velocity and property variations. Temperature has smooth distributions near the wall although there is large variation of properties near the pseudocritical point. Temperature profiles develop faster in upward flow than in no gravity flow because of the increase in turbulent transport due to buoyancy effect. When velocity near the wall reaches a maximum in upward flow, the temperature below the pseudocritical point has a steep gradient in the radial direction. This is due to the decrease of turbulent diffusivity based on velocity gradient and turbulent heat transfer becomes negligible at this point.

Buoyancy force due to density variation produces quite different distributions of shear stress in the tube. Figure 8 shows the comparison of shear stress distributions along the tube for no-gravity flow and upward flow. For no-gravity flow, the shear stress is almost linear with radius although there is steep variation near the wall. For upward flow, the shear stress is positive near the wall and negative in the central region due to the M-shaped velocity profile developing along the vertical tube. With the steep velocity gradient near the wall, shear stress and turbulent viscosity decrease very fast radially compared

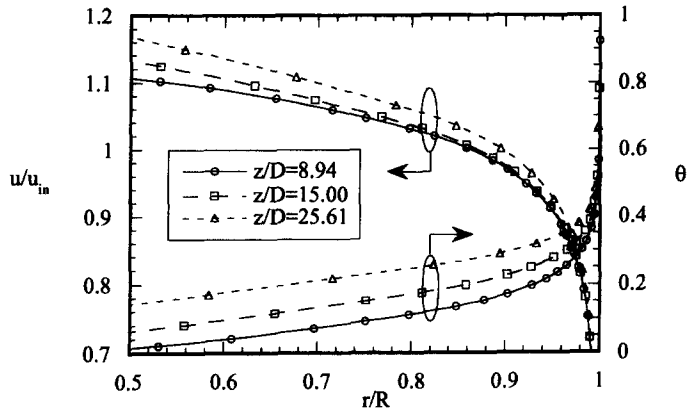

Fig. 6. Velocity and temperature distributions along the tube for no-gravity flow of water: $P = 24$ MPa; $Re = 10^5$; $T_{in} = 638$ K; $T_w = 668$ K.

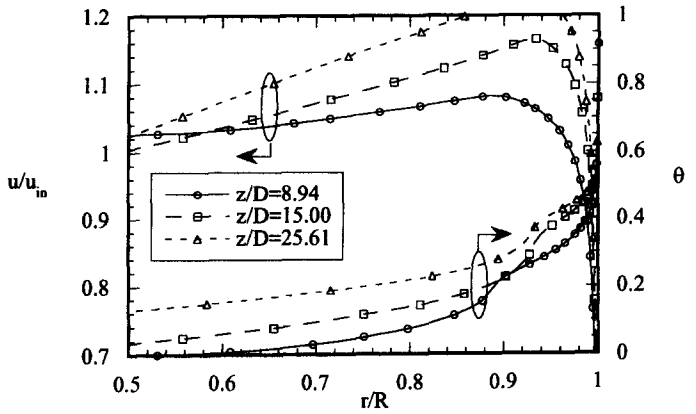

Fig. 7. Velocity and temperature distributions along the tube for upward flow of water: $P = 24$ MPa; $Re = 10^5$; $T_{in} = 638$ K; $T_w = 668$ K.

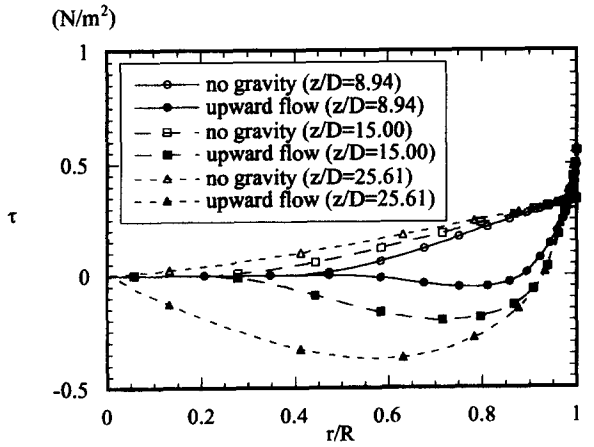

Fig. 8. Shear stress distribution along the tube: $P = 24$ MPa; $Re = 10^5$; $T_{in} = 638$ K; $T_w = 668$ K.

with no-gravity flow. Many studies show that this M-shaped velocity is related to the heat transfer deterioration by laminarization near the wall and resulting reduction in turbulence generation. The point where the velocity has peak value and the gradient is zero near the wall suppresses turbulent transport in the boundary layer region as for the temperature distribution.

Turbulent viscosity is composed of a value based on the standard mixing length model and a ratio term

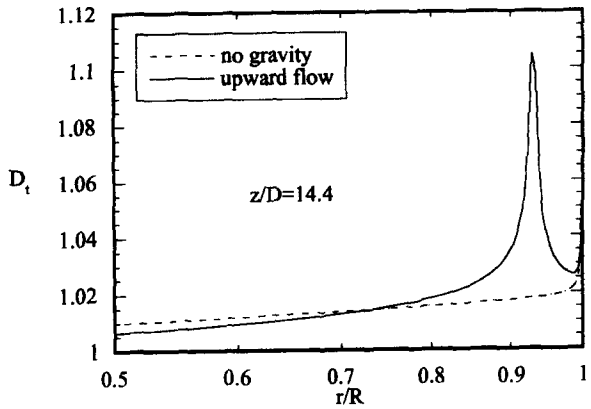

Fig. 9. Turbulent viscosity ratio distribution: $P = 24$ MPa; $Re = 10^5$; $T_{in} = 638$ K; $T_w = 668$ K.

which includes the effect of density fluctuation on turbulent transport. Figure 9 shows the ratio between the values of turbulent viscosity based on the standard two layer mixing length model and the modified model for upward and no-gravity flow. This ratio is:

$$D_t = 1 - \left(\frac{\bar{\beta}}{C_p}\frac{1}{Pr_t}\frac{\partial \bar{i}}{\partial y}\right) - \left(\frac{\bar{\beta}}{C_p}\frac{1}{Pr_t}\frac{\partial \bar{i}}{\partial y}\right)^2. \quad (32)$$

For no-gravity flow, the ratio has a value of 1.05 near the wall and far from the peak the ratio is less than 1.02. The ratio depends on compressibility, mixing length and enthalpy gradient, and the small peak at the wall is due to the large variation of properties, especially compressibility. For upward flow, there is a large peak in the ratio of turbulent viscosities located near the zero velocity gradient point. This peak is related to the temperature gradient, which is very steep due to the low turbulent viscosity resulting from the zero velocity gradient. The large temperature gradient produces relatively large fluctuations of density. Thus, this ratio increases the value of turbulent viscosity near the zero velocity gradient of the M-shaped velocity caused by buoyancy.

Property variations near the critical region affect heat transfer in the tube and they are also coupled with momentum transfer. Figure 10 shows the comparison of heat transfer coefficient distributions along the tube for three inlet Reynolds numbers with and without gravity force. As the Reynolds number increases, the difference in heat transfer coefficient between upward flow and no gravity becomes smaller. For high Reynolds number ($Re \simeq 5 \times 10^5$), and no-gravity flows, the heat transfer coefficient decreases gradually and there is a slight increase in heat transfer coefficients along the tube after passing the entrance region ($z/D > 15$). This slight increase in heat transfer coefficients is due to small acceleration of fluid near the wall based on the decrease of density and viscosity. But for upward flow, the heat transfer coefficient increases after a shorter distance ($z/D > 3$) from the inlet for Reynolds numbers of 5×10^4 and 10^5. This increase in heat transfer coefficient is related to the increase of bulk temperature and wall heat flux along the tube. Due to fluid acceleration near the wall by the buoyancy effect, the large velocity gradient near the wall increases turbulent transport. The buoyancy effect due to gravity force with density variation has larger influence on heat transfer than the effect of acceleration which results from the decrease in density and viscosity near the wall. Deterioration in heat transfer due to the gravity force appears in local temperature distributions with steep gradients. But there is no deterioration phenomena in heat transfer coefficients or wall heat flux along the tube in these upward flows.

Figure 11 shows the heat transfer coefficient distribution along the tube for upward flow for three inlet pressures. Heat transfer coefficients decrease near the inlet region of the tube and then increase along the tube. The locations of heat transfer coefficient increase depend on the pressure in the tube. As the pressure approaches the critical point, the pseudocritical temperature approaches the critical temperature and the peak value of specific heat at the pseudocritical temperature increases. Buoyancy force (Grashof number) in the tube also increases. Large turbulent transport near the wall due to high specific heat and large buoyancy effect result in heat transfer coefficients.

Friction factor distributions for these pressure conditions are also shown in Fig. 11. The friction factor is calculated from:

$$f = \frac{8\tau_w}{\rho_{in} u_{in}^2}. \quad (33)$$

It decreases near the entrance region like the heat transfer coefficient, and then increases along the tube due to the buoyancy effect at the tube wall. The friction factor increases slowly in the region of $z/D > 15$. Compared with heat transfer coefficient distributions along the tube, locations where friction factors start to increase are close to the entrance. As the pressure approaches the critical point, the minimum in friction factor becomes lower and the location of increase rate

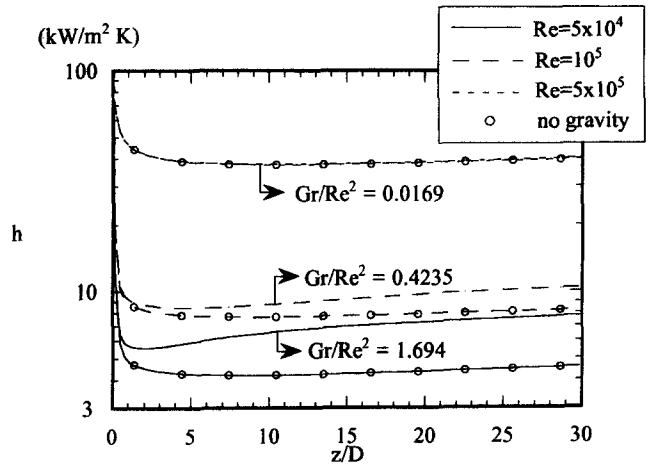

Fig. 10. Heat transfer coefficient distribution for various Reynolds numbers: $P = 24$ MPa; $T_{in} = 638$ K; $T_w = 668$ K.

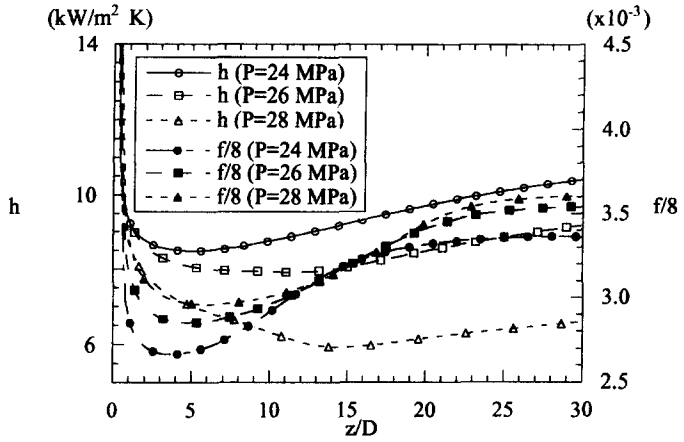

Fig. 11. Heat transfer coefficient and friction factor distribution for various inlet pressures: $Re = 10^5$; $T_{in} = 638$ K; $T_w = 668$ K.

change becomes closer to the entrance. Although the velocity gradient at the wall increases due to the buoyancy force with the decrease of pressure, the decrease of fluid viscosity at the wall produces lower wall shear stress.

Near the critical region, property variations depend strongly on pressure as well as temperature. Buoyancy effects in the vertical tube are usually represented by the parameter [22] of Gr/Re^2 while Hall [4] suggests $Gr/Re^{1.8}$, and Jackson and Hall [23] recommend $Gr/Re^{2.7}$ as the criterion parameter for buoyancy. The Grashof number based on inlet values is:

$$Gr = \frac{g(\rho_b - \rho_w)D^3}{\rho_b \nu_b^2}. \quad (34)$$

Table 2 shows the values of the buoyancy parameter for several pressures. For 24 MPa, the parameters are 0.424, 4.235, and 1.339×10^4, respectively. The buoyancy effect cannot be neglected as can be seen in the velocity profile distributions. As the pressure approaches the critical pressure ($P_c = 22.05$ MPa), $Gr/Re^{1.8}$ increases due to the large density gradient (compressibility) near the pseudocritical point. It can be seen that the buoyancy parameter, $Gr/Re^{1.8}$ is about

Table 2. Values of buoyancy parameters for several pressures; $Re = 10^5$, $T_{in} = 638$ K, $T_w = 668$ K

Pressure	Gr/Re^2	$Gr/Re^{1.8}$	$Gr/Re^{2.7}$
23 MPa	0.4418	4.418	1.397×10^{-4}
24 MPa	0.4235	4.235	1.339×10^{-4}
26 MPa	0.3658	3.658	1.157×10^{-4}
28 MPa	0.2539	2.539	8.029×10^{-5}
30 MPa	0.1736	1.736	5.490×10^{-5}

1.7 times higher at 24 MPa than at 28 MPa. Thus, the fluid near the wall accelerates much faster for 24 MPa.

Hall [4] uses the buoyancy effect criterion:

$$Gr/Re^{1.8} < 10^{-1} \tag{35}$$

and Shiralkar and Griffith [24] suggest the following:

$$Gr/Re^{2} < 10^{-2}. \tag{36}$$

The criterion suggested by Jackson and Hall [23] is:

$$Gr/Re^{2.7} < 10^{-5}. \tag{37}$$

Values of Gr/Re^2 are shown in Fig. 10 for heat transfer coefficient distributions along the tube. They show that every criterion is reasonable in estimating when buoyancy becomes important in affecting the heat transfer coefficient. The parameters of Gr/Re^2 at 24 MPa and 26 MPa are about 67 and 44% higher than at 28 Mpa. The heat transfer coefficient increases more rapidly as the pressure approaches the critical pressure due to these effects as in Fig. 11.

5. CONCLUSIONS

Numerical calculations based on the mixing length model are performed for upward flow in the entrance region of a vertical tube near the critical point for water and CO_2. The mixing length model adopted here includes the effect of density fluctuation on turbulent diffusivity and it is shown to predict differences of up to 10% in turbulent diffusivity over the standard mixing length model. The numerical results are compared with experimental data and results using the k–ε turbulence model. Predictions using the mixing length model are in agreement with trends in the experimental data. It is found that the highly coupled fluid flow and heat transfer caused by the large property variations near the pseudocritical point cause a slow approach to fully developed conditions. Property variations near the pseudocritical point affect both the fluid flow and heat transfer. Steep gradients in density produce large buoyancy forces which cannot be neglected even at $Re_{in} = 10^5$ in the vertical tube, and this buoyancy force has larger influence on momentum and heat transfer compared with bulk fluid acceleration due to the density and viscosity variations. The buoyancy effect parameter depends on the fluid pressure as well as temperature because of pressure effects on density variation. For upward flow, the heat transfer coefficient increases after some distance from the entrance for constant wall temperature for inlet fluid temperatures below the pseudocritical temperature. This increase depends on the fluid pressure.

The strong coupling of the heat transfer and fluid velocity through the pressure- and temperature-dependent properties implies that no simple correlation in terms of traditional dimensional parameters can be expected to give useful predictions except over very limited ranges. Thus, design of process equipment operating at near critical conditions may require complete numerical analysis for adequate prediction of behavior.

REFERENCES

1. Jones, W. P. and Launder, B. E., The prediction of laminarization with a two-equation model of turbulence. *International Journal of Heat and Mass Transfer*, 1972, **15**(2), 301–314.
2. Bellmore, C. P. and Reid, R. L., Numerical prediction of wall temperatures for near critical para-hydrogen in turbulent upflow inside vertical tubes. *Journal of Heat Transfer*, 1983, **105**(3), 536–541.
3. Popov, V. N. and Valueva, E. P., Heat transfer and turbulent flow of water at supercritical parameters of state in a vertical tube with a significant effect of free convection. *Teploenergetika*, 1986, **33**, 22–29.
4. Hall, W. B., Heat transfer near the critical point. *Advances in Heat Transfer*, 1971, **7**, 1–83.
5. Koshizuka, S., Takano, N. and Oka, Y., Numerical analysis of deterioration phenomena in heat transfer to superficial water. *International Journal of Heat and Mass Transfer*, 1995, **38**(16), 3077–3084.
6. Zhou, N. and Krishnan, A., Laminar and turbulent heat transfer in flow of supercritical CO_2. *Proceedings of the 30th National Heat Transfer Conference*, Vol. 5. ASME, Portland, OR, 1995, pp. 53–63.
7. Grief, R., An experimental and theoretical study of heat transfer in vertical tube flows. *Journal of Heat Transfer*, 1978, **100**(1), 86–91.
8. Van Driest, E. R., On turbulent flow near a wall. *Journal of Aerospace Science*, 1956, **23**, 1007–1011.
9. Schlichting, H., *Boundary Theory*, 7th edn. McGraw-Hill, New York, 1979.
10. Kays, W. M. and Crawford, M. E., *Convective Heat and Mass Transfer*, 3rd edn. McGraw-Hill, New York, 1993.
11. Lester, H., John, S. G. and George, S. K., *Steam Tables*. Hemisphere, New York, 1984.
12. Hendricks, R. C., Baron, A. K. and Peller, J. C., GASP–a computer code for calculating the thermodynamic and transport properties for ten fluids. NASA Technical Note D-7808, 1975.
13. Patankar, S. V., *Numerical Heat Transfer and Fluid Flow*. Hemisphere, Washington, DC, 1980.
14. Wood, R. D. and Smith J. M., Heat transfer in the critical region—temperature and velocity profiles in turbulent flow. *AIChE Journal*, 1964, **10**(2), 180–186.
15. Goldmann, K., Heat transfer to supercritical water and other fluids with temperature dependent properties. *Chemical Engineering Progress Symposium*, 1954, **50**(11), pp. 105–113.
16. Sastry, V. S. and Schnurr, N. M., An analytical investigation of forced convection heat transfer to fluids near the thermodynamic critical point. *Journal of Heat Transfer*, 1975, **97**(2), 226–230.
17. Yamagata, K., Nishikawa, K., Hasegawa, S., Fujii, T. and Yoshida, S., Forced convective heat transfer to supercritical water flowing in tubes. *International Journal of Heat and Mass Transfer*, 1972, **15**(12), 2575–2593.
18. Dittus, F. W. and Boelter, L. M. K., Heat transfer in automobile radiators of tubular type. *University of California Publications in Engineering*, 1930, **2**(13), 443–461.
19. Swenson, H. S., Carver, J. R. and Kakarala, C. R., Heat transfer to supercritical water in smooth bore tubes. *Journal of Heat Transfer*, 1965, **87**(4), 477–484.
20. Kurganov, V. A. and Ankudinov, V. B., Calculation of normal and deteriorated heat transfer in tubes with turbulent flow of liquids in the near critical and vapor region of state. *Teploenergetika*, 1985, **32**, 53–57.

21. Petukhov, B. S. and Polyakov, A. F., *Heat Transfer in Turbulent Mixed Convection*. Hemisphere, New York, 1988.
22. Polyakov, A. F., Heat transfer under supercritical pressures. *Advances in Heat Transfer*, Academic Press, San Diego, CA, 1991, **21,** 1–50.
23. Jackson, J. D. and Hall, W. B., Influences of buoyancy on heat transfer to fluids flowing in vertical tubes under turbulent conditions. *Turbulent Forced Convection in Channels and Bundles*. Hemisphere, New York, 1979, pp. 613–640.
24. Shiralkar, B. and Griffith, P., The effect of swirl, inlet conditions, flow direction, and tube diameter on the heat transfer to fluids at supercritical pressure. *Journal of Heat Transfer*, 1970, **92**(3), 27–36.